Adsorption 2, 9–21 (1996)


# The Effect of Nanopore Shape on the Structure and Isotherms of Adsorbed Fluids

D. KEFFER, H. TED DAVIS AND ALON V. McCORMICK
*Department of Chemical Engineering and Materials Science, University of Minnesota, 421 Washington Avenue SE, Minneapolis, MN 55455*

**Abstract.** A Grand Canonical Monte Carlo simulation method is used to determine the adsorption isotherms, interaction energies, entropies, and density distribution of a Lennard-Jones fluid adsorbed in smooth-walled nanopores of varying size and shape. We specifically include very crowded pores, where packing effects are important. Differences in the isotherms of slit, cylindrical, and spherical nanopores of varying sizes can be explained in terms of the adsorbate-adsorbate interaction energy, the adsorbate-pore interaction energy, and the density profiles, which influence the balance between the former and the latter energy contributions. The expectation from low loading studies that the most energetically favorable adsorbate-pore interactions maximize adsorption is not borne out at intermediate and higher loadings. Instead, the relationships between adsorbed amounts and pore size and shape are found to be strong functions of the depth and steepness of the external potential, the extent to which adsorbate-adsorbate repulsion establishes short range fluid order, and the accessible pore volume. This study has implications for high pore density processes in nanoporous materials, such as zeolite catalysis, separations, and templating in zeolite synthesis.

**Keywords:** nanopores, zeolites, Monte Carlo simulations

## 1. Introduction

Much research has been performed using Molecular Dynamics (MD) and Monte Carlo (MC) computer simulations to study the behavior of fluids in idealized nanopore systems. Simulations have been used to study fluids adsorbed in slit pores (Sarman, 1990; Somers and Davis, 1992; Murad et al., 1993; Han et al., 1993; Tan and Gubbins, 1992; Somers et al., 1993; Schoen et al., 1989; Jiang et al., 1993), cylindrical pores (Macelroy and Suh, 1987, 1989; Groot et al., 1987; Antonchenko et al., 1988; Bratko et al., 1989; Heinbuch and Fischer, 1987; Glandt, 1980; Derouane and Lucas, 1988; Peterson et al., 1986; Peterson and Gubbins, 1987; Walton and Quirke, 1989; Saito and Foley, 1990; Demi, 1991), and spherical pores (Macpherson et al., 1987; Carignan et al., 1988; Dunne and Myers, 1994).

The major aim of the study of idealized nanopores is to establish the relationships between adsorbate-nanopore system parameters—namely, pore shape, pore size, and adsorbate chemical potential—and the resulting system properties—namely, density distributions, adsorption isotherms, and diffusivities. Once such relationships are understood in simple systems, one can better predict adsorption in real, more complex nanopores, e.g., in zeolites. Simple systems also provide useful challenges for the development of theoretical approaches, using either density functional theory or integral equations resulting from the closure of either the Yvon-Born-Green Hierarchy or the Ornstein-Zernike Equation. Likewise, we limit our attention here to simple Lennard-Jones fluids, thereby isolating the effects due to nanopore shape and size.

The interpretation of previous simulations is varied and sometimes contradictory. It has been postulated that adsorption heats should increase monotonically as the ratio of pore diameter to adsorbate diameter approaches unity, i.e., as a better fit is achieved (Derouane and Lucas, 1988). Also, it has been stated that as the

curvature of the pore increases, the adsorption heats can increase by as much as a factor of 8. Such a view has provided valuable insight into tasks including Xe NMR chemical shifts, predicting sorption selectivities in separations and catalysis, and predicting suitable templates for zeolite synthesis. However, previous work showing inhomogeneous packing among fluids in confined spaces, e.g., (Somers and Davis, 1992), leads us to suspect that this straightforward behavior will become more complicated at high density. Indeed, we demonstrate in this work that these trends change markedly at high loadings.

Glandt and coworkers compared the density of an adsorbed hard-sphere fluid phase inside slit, cylindrical, and spherical pores in equilibrium with the same bulk fluid phase at a given pore size and bulk fluid density (Glandt, 1980). We seek here to fully explore the preferences of adsorption for pore shape over a wide range of pore sizes and chemical potentials.

We use the density profiles, energies, and entropies of the adsorbate fluid within the pore to explain the trends we observe in the relationship between adsorption and pore size and curvature. In addition, we use Grand Canonical (constant volume, chemical potential, and temperature) MC methods to determine this relationship as a function of chemical potential.

Because it is strongly inhomogeneous in nanopores, fluid structure should play an important role in adsorption. Furthermore, we might expect the adsorption trends to change non-monotonically with loading or chemical potential. At low loadings, we verify the preference for adsorption in pores that better "fit" the adsorbate molecules. At high loadings, though, we will find that this relationship is more complex than previously thought. Even so, this complex behavior can be rationalized in terms of (1) the depth and steepness of the external potential, (2) the ability to establish short range fluid order, and (3) the volume accessible to the adsorbate.

## 2. Grand Canonical Monte Carlo

The equilibrium criterion in the grand canonical ensemble is to minimize the grand potential, defined as

$$\Omega(\mu, V, T) = U - TS - N\mu \tag{1}$$

where $U$ is the energy, $T$ is the temperature, $S$ is the entropy, $N$ is the number of adsorbate molecules, and $\mu$ is the chemical potential.

For each grand canonical ensemble simulation, we typically ran about 1,000,000 to 1,500,000 steps and discarded the first 500,000. The steps were equally divided between translations, insertions, and deletions. The translations were kept at a 50% acceptance rate by varying the size of the step. The insertion and deletion acceptance rates were allowed to vary depending on loading. As is typical of MC particle insertion/deletion methods in high density fluids, the insertion and deletion acceptance rates were far lower at high loadings.

The algorithm for GCMC is as follows. Random initial positions are assigned to $N_{\text{ads}}$ adsorbates. The net potential due to adsorbate-adsorbate and adsorbate-pore wall interactions is calculated. At random, one of the adsorbates is chosen to be translated, inserted, or deleted. The distances of the translation in each of the $x$, $y$, and $z$ directions are randomly picked from a range of 0 to $\delta$, where a small, intial $\delta$ is specified. The energy of the system is recalculated with the new position of the translated molecule. The difference between the new and old potential energy of the system is $\delta U_{\text{pot}}$. The translation is accepted according to the following probability: (Allen and Tildesley, 1987)

$$\text{Prob} = \begin{cases} 1 & \text{if } \delta U < 0 \\ \dfrac{-\delta U}{e^{kbT}} & \text{if } 0 > \delta U > \delta U_{\max} \\ 0 & \text{if } \delta U > \delta U_{\max} \end{cases} \tag{2}$$

In the case of an insertion or deletion, the total change in energy is given by

$$\delta U_{\text{ins}} = \delta U - \mu + \ln\left(\frac{(N+1)\Lambda^3}{V}\right) \tag{3a}$$

or

$$\delta U_{\text{del}} = \delta U + \mu - \ln\left(\frac{N\Lambda^3}{V}\right) \tag{3b}$$

where $\delta U$ is the change in adsorbate-adsorbate and adsorbate-pore potentials due to the inserted or deleted atom, $\mu$ is the chemical potential, $N$ is the number of adsorbates, $V$ is the volume of the system, and $\Lambda$ is the de Broglie thermal wavelength. As was the case for a translation, the net potential energy of the system after the insertion or deletion is computed and compared to the previous energy. The move is accepted with the probability given in Eq. 2. The procedure is repeated until the net energy and the number of adsorbates in the system fluctuate about a constant average, at which point accumulation of data begins.

The adsorbate-adsorbate potential was taken as a Lennard-Jones potential,

$$U_{ij} = 4\varepsilon_{aa}\left[\left(\frac{\sigma_{aa}}{r_{ij}}\right)^{12} - \left(\frac{\sigma_{aa}}{r_{ij}}\right)^{6}\right] \quad (4)$$

with parameters representative of Xenon, $\sigma_{aa} = 4.2$ Å and $\varepsilon_{aa}/k = 221$ K. In this work, we confine our attention to simple Lennard-Jones molecules in the interests of isolating the effects of pore size and shape and in the interests of economic use of computational resources. It is the first step in capturing the experimental high density behavior of more complicated molecules, e.g., templates or reaction intermediates. We include adsorbate-adsorbate interactions over all pairs; we do not use a cut-off distance for the potential. (We have found that when dealing with less than 200 molecules, higher computation speed is obtained on a Cray-XMP (with a 64-element vector register) without a cut-off distance or neighbor list because the FORTRAN IF-THEN structures required by the regular updating of the neighbor list prevent the vectorization of the DO-LOOPS, resulting in a net decrease in computational efficiency.)

The adsorbate pore potential was taken as a Lennard-Jones potential integrated over the entire solid volume outside the slit, cylindrical, and spherical pores. We limit our investigation to pores with smooth walls having no atomistic detail. The adsorbate pore potential parameters were $\sigma_{ap}/\sigma_{aa} = 1.0$ and $\varepsilon_{ap}/\varepsilon_{aa} = 1.5$ with a solid density $\rho_s = 1.0$ molecules/$\sigma_{aa}^3$. The forms of the potential between the $i$th adsorbate and the pore is a 9-3 potentials,

$$U_{ip} = 4\rho_s\varepsilon_{ap}\left[c_9\left(\frac{\sigma_{ap}}{r_i}\right)^{9} - c_3\left(\frac{\sigma_{ap}}{r_i}\right)^{3}\right] \quad (5)$$

representing pores in semi-infinite solids rather than thin-walled pores. The constants $c_9$ and $c_3$ are determined by the geometry of the pore and $r_i$ is either the perpendicular distance to the walls (for slit pores) or the radial distance from the center of the pore (for cylindrical and spherical pores). For the cylindrical and spherical pores, $c_9$ and $c_3$ are calculated numerically (Peterson and Gubbins, 1987). Again, we do not use cut-off distances for the potential. We find qualitative agreement when comparing the density distributions of a slit pore with a 9-3 potential to those of a 10-4-3 potential (Somers and Davis, 1992).

The width of the pores are measured from the plane where the L-J external potential diverges at one side of the pore to the same plane on the opposite side. This represents the distance between centers of the first layer of atoms on opposite walls.

The area of the slit, the length of the cylindrical, and the number of spherical pores were chosen to yield the desired volume within the pore. For all simulations, we chose a pore volume which yielded an average value of $N_{\text{ads}}$ of about 150 molecules. Standard periodic boundary conditions and minimum image conventions were applied across those boundaries.

The density distributions were obtained by dividing the pores into 100 bins—planar bins in the case of the slit pore, annular bins in the case of the cylindrical pore, and spherical shells in the spherical pore—and counting the occupancy in each bin. Sampling was performed every 100 steps during data production and then averaged at the end of the run. The potential energy was calculated every time step and averaged at the end of the run.

Entropies were calculated using Eq. (1) and substituting $\langle U_{\text{pot}}\rangle + 3/2\langle N\rangle kT$ for $U$ where $\langle U_{\text{pot}}\rangle$ is the ensemble average of the total potential energy, including adsorbate-adsorbate and adsorbate-pore interactions, and where the grand potential was calculated numerically: (Van Tassel et al., 1993)

$$\Omega = \int_{-\infty}^{\mu}\left(\frac{\partial\Omega}{\partial\mu}\right)_{V,T} d\mu' = \int_{-\infty}^{\mu}(-\langle N\rangle)\, d\mu' \quad (6)$$

where $\langle N\rangle$ is the ensemble average of adsorbate molecules at chemical potential $\mu'$.

## 3. Results and Discussion

### A. *Slit Pore*

In Fig. 1, we present the adsorption isotherms for Lennard-Jones xenon in slit pores of width 2.0, 2.5, and $3.2\sigma_{aa}$. We chose these pore widths because they are close to the pore dimensions of various zeolites and because different numbers of molecular layers are anticipated inside the pores (Somers and Davis, 1992). We found two overlapping layers of high density of adsorbates in the slit pore of width $2.0\sigma_{aa}$, two distinct layers in the pore of width $2.5\sigma_{aa}$, and three distinct layers in the pore of width $3.2\sigma_{aa}$. (Figs. 2a,c)

We gauge the favorability for adsorption by the average adsorbate density within the total pore volume.

At *low* chemical potential, the *smaller* slit pore most favors adsorption. At *high* chemical potential, though,

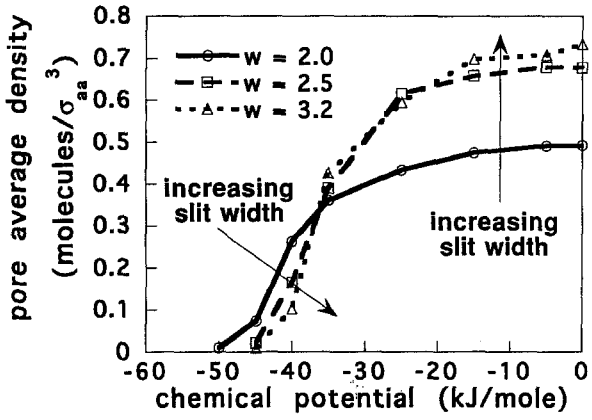


*Figure 1.* Isotherms for slit pores of width 2.0, 2.5, and $3.2\sigma_{aa}$ at $T = 300$ K.

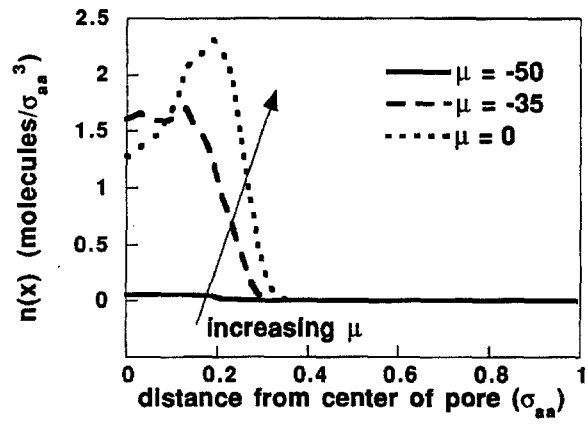


(a)

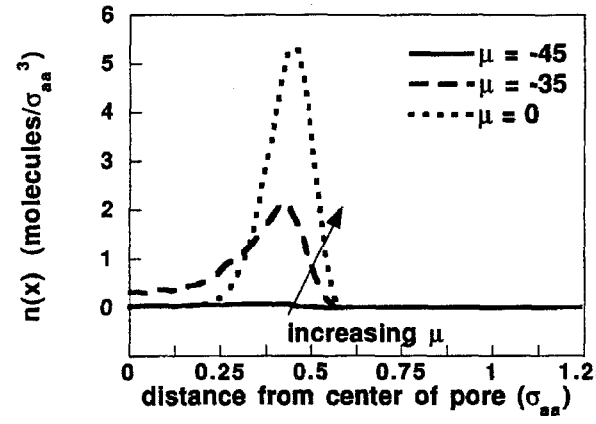


(b)

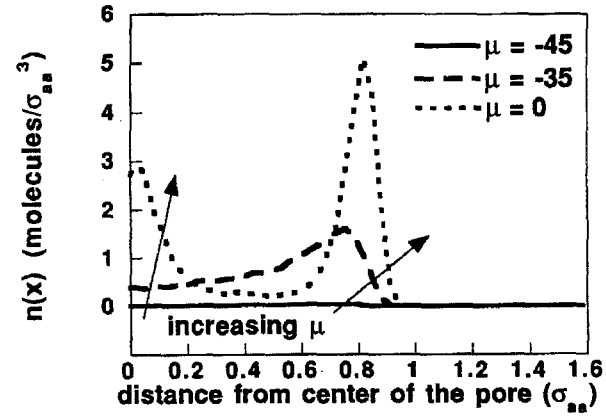


(c)

*Figure 2.* Density profiles in slit pores for several values of the chemical potential. (a) Slit width = $2.0\sigma_{aa}$, (b) slit width = $2.5\sigma_{aa}$, (c) slit width = $3.2\sigma_{aa}$.

the *larger* pore most favors adsorption. The reversal of preference can be explained with reference to the interaction energies and entropies, shown in Figs. 3(a,b) and 4(a,b). The total intensive, total extensive, adsorbate-adsorbate (*aa*), and adsorbate-pore (*ap*) interaction energies all vary with the chemical potential. We define intensive properties to be per molecule, i.e., system size independent. Extensive properties are system size dependent and, for comparison between pores, have been scaled to systems of equal pore volume (1 mole of $\sigma_{aa}^3$ volume elements.) The intensive properties reflects the status of an individual molecule while the extensive properties are important in minimizing the grand potential of Eq. 1. It is important to show both the intensive and extensive interaction energies (Figs. 3(a, b)) because there can be situations where the energy per adsorbate may increase while the extensive energy continues to decrease. The intensive and extensive entropies are shown in Figs. 4(a,b).

The adsorption behavior is qualitatively different at low and high loadings.

*a. Low Loadings ($\mu \leq -45$ kJ/mole).* At low loadings, the adsorbates simply occupy the energetically most favorable positions in the pore. The intensive total energy is most favorable in the smallest pore (Fig. 4(a)) simply because in this pore the attractive potentials due to each wall best overlap, making the deepest energy well (Fig. 3(a)). The *aa* interaction (Fig. 3(b)) is considerably smaller than the *ap* interaction at these low chemical potentials.

The intensive entropy is most favorable in the largest pore because the adsorbates reside in a wider, less

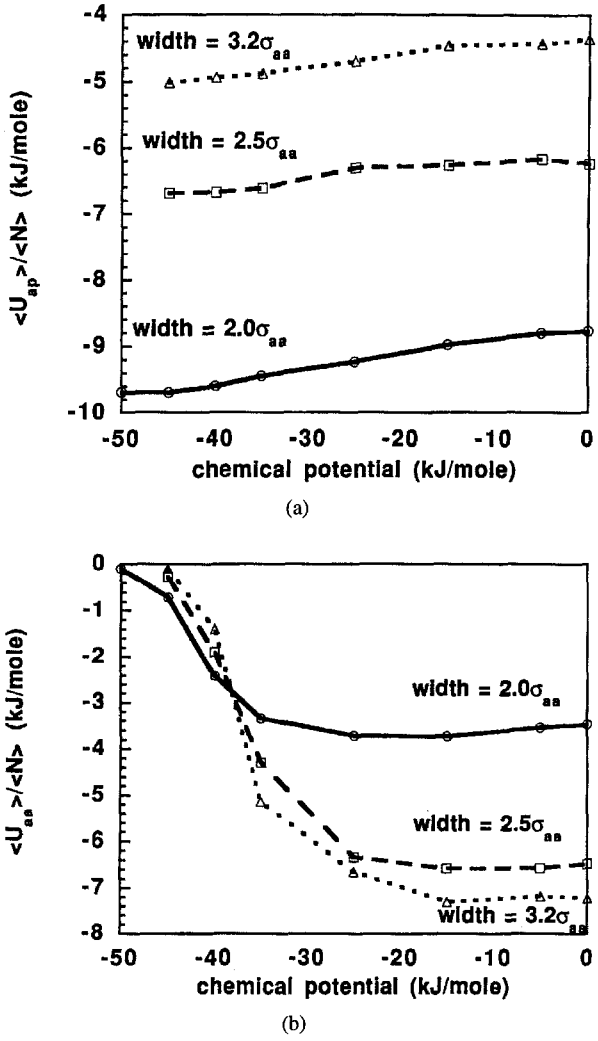


*Figure 3.* Interaction energies in slit pores as a function of chemical potential. (a) Intensive adsorbate-adsorbate interaction energy, (b) intensive adsorbate-pore interaction energy.

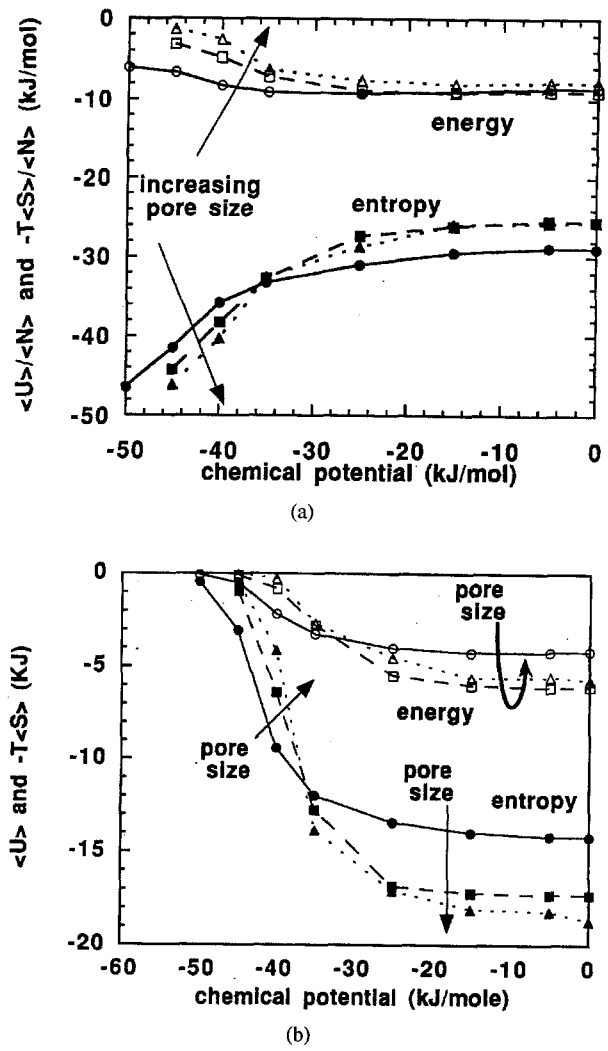


*Figure 4.* Energetic and entropic contributions in slit pores as a function of chemical potential. (a) Intensive energetic and entropic terms, (b) extensive energetic and entropic terms.

steeply bounded external potential well and so have available to them a greater volume of the pore. Nevertheless, the extensive entropy is more favorable for smaller pores since there are more adsorbates. The entropic advantage of large pores fails to be manifest at low chemical potential.

*b. High Loadings ($\mu \geq -15$ kJ/mole).* At high loadings, the density profiles (Fig. 2(a,c)) show layers of adsorbates that become more distinct and more numerous (though smaller in magnitude) in the larger pores. This layering is a result of the ability to pack efficiently in the pore at high loadings. Although the *ap* attraction (Fig. 3(a)) is most favorable in the smallest pore, greater adsorption now occurs in the larger pore. This reversal cannot be explained solely in terms of the *aa* energetic attraction (Fig. 3(b)) since the energy contribution only slightly favors the larger pore and does not do so enough to reverse the total energy trend (Fig. 4(a)) from that at low loading. Instead, the entropic trends must now be important.

At high loadings, the intensive entropy is greatest in the smallest pore because the size of the pore prevents the formation of distinct layers. The more distinct layers in the larger pores indicate a more structured fluid, tending to produce a lower intensive entropy. However,

we see that the entropy does not decrease monotonically. In fact, at high loading, the entropy of the $3.2\sigma_{aa}$ pore is no lower than that of the $2.5\sigma_{aa}$ pore. The important point is that entropy is more favorable in the large pore than we might have expected. Thus the largest pore adsorbs more.

*c. Energetic versus Entropic Effects.* The relative importance of the energetic and entropic contributions to adsorption changes with loading. The intensive energetic ($U$) and entropic ($-T\langle S\rangle$) terms are plotted in Fig. 4(a).

At low loading, the energetic term favors adsorption in the smallest pore but the entropic term favors the largest pore. The smallest pore adsorbs more, though not as much more as might be expected since entropy opposes it.

At high loading, though both the intensive energetic and entropic terms favor the smallest pore, both the extensive entropy and energy favor the larger pores. The difference here is due to the differences in density inside the three pores. Though the average state of a single adsorbate remains more favorable in the smaller pore, the intensive properties fail to account for the greater accessible volume in the larger pore, which allows better packing of the adsorbates per unit volume.

The trend in the isotherms correlates most closely to the extensive entropic term. At high loadings, adsorption is strictly greater with increasing pore width despite the fact that the total extensive energy (Fig. 4(b)) does not monotically favor a larger pore size. We will see that this effect is even more pronounced in the cylindrical and spherical pores.

## B. *Cylindrical Pores*

We now present analogous data for the cylindrical pore. Figure 5 plots the adsorption isotherms of Xe in cylindrical pores of diameters 2.0, 2.5, and $3.2\sigma_{aa}$. Fig. 6(a,c) shows the density profiles in those pores at several chemical potentials. Figure 7(a,b) shows the $ap$ and $aa$ interaction energies. The intensive and extensive total energy and entropy in the three pores as a function of chemical potential are shown in Fig. 8(a,b).

*a. Low Loadings ($\mu \leq -45$ kJ/mole).* At low loadings, we find that adsorption is favored in the smaller cylindrical pores, as was the case for the slit pores, because the $ap$ interactions are most favorable in the smaller pore (Fig. 7(a)); the $aa$ interactions are

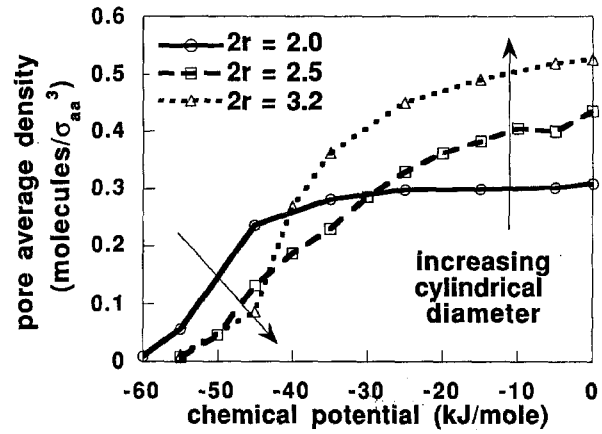


*Figure 5.* Isotherms for cylindrical pores of diameter 2.0, 2.5, and 3.2 $\sigma_{aa}$ at $T = 300$ K.

negligible (Fig. 7(b)). Again, this occurs in spite of the fact that the intensive entropy increases with increasing cylindrical pore diameter, reflecting the greater volume explored.

Comparing the cylindrical pore isotherms to those of the slit pore, we find as expected (Glandt, 1980), that the cylindrical pore is favored over the slit pore at low loadings because the external potential ($ap$) well depth is greater in the cylindrical pore, which in turn is due to the curvature of the cylindrical pore walls.

*b. High Loadings ($\mu \geq -15$ kJ/mole).* The density distribution in the smallest pore remains constant at high chemical potentials (Fig. 6(a)). In the larger pores, though, the layering becomes sharper with increasing chemical potential. The peaks in the density profile continue to narrow and heighten (Fig. 6(b,c)).

As was the case for the slit pores, the relation between adsorption and pore size has reversed from that of low loadings. Again, the $aa$ attraction increases with loading most rapidly in the larger pores (Fig. 7(b)). The $ap$ interaction is relatively constant at high chemical potentials in the pores of diameter 2.0 and $3.2\sigma_{aa}$ but becomes less attractive at $2.5\sigma_{aa}$ (Fig. 7(a)) because in this pore the molecules can neither form a peak in the center of the pore (as is the case in the smaller pore) nor form an annular region of high density as favorable as that in the larger pore.

As was the case for slit pores, the intensive entropy decreases for larger pores, tending to oppose the preference for larger pores (Fig. 8(a)).

At high chemical potential, we find the density inside the cylindrical pore is less than that in the comparable

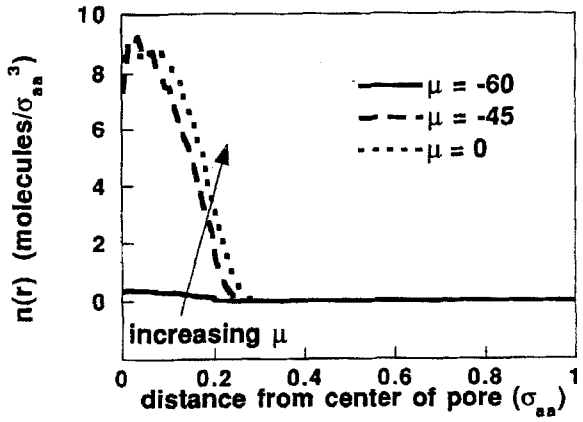


(a)

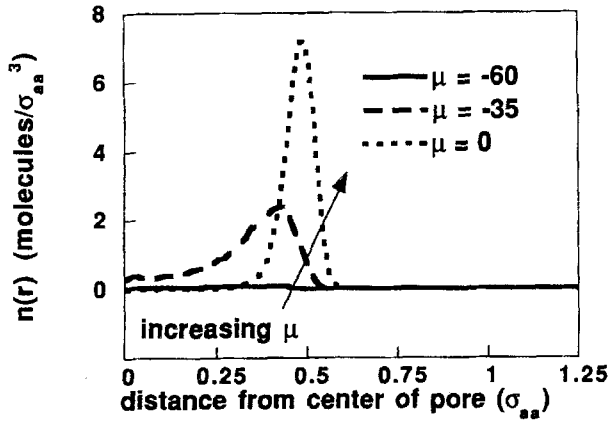


(b)

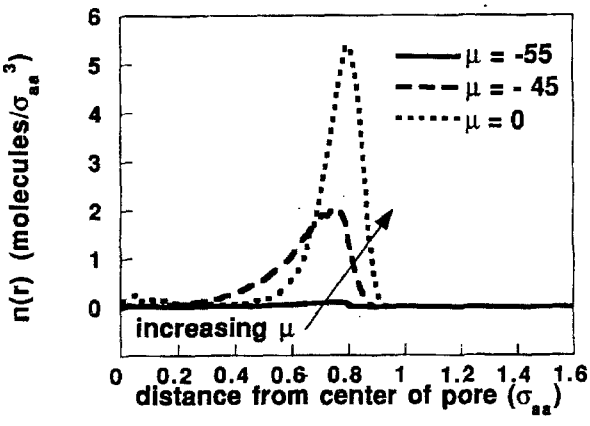


(c)

*Figure 6.* Radial density profiles in cylindrical pores for several values of the chemical potential. (a) Cylindrical diameter = $2.0\sigma_{aa}$, (b) cylindrical diameter = $2.5\sigma_{aa}$, (c) cylindrical diameter = $3.2\sigma_{aa}$.

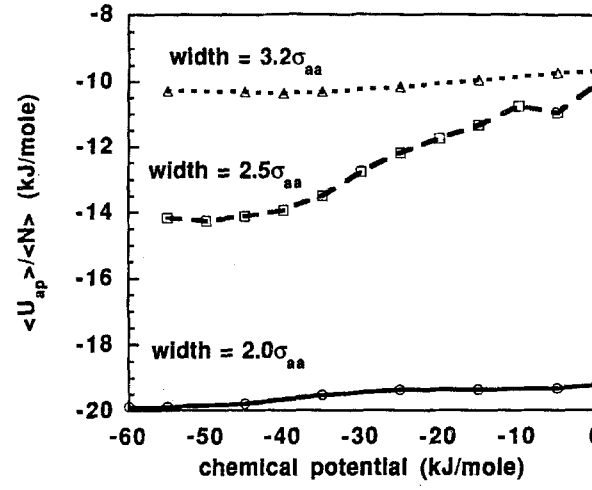


(a)

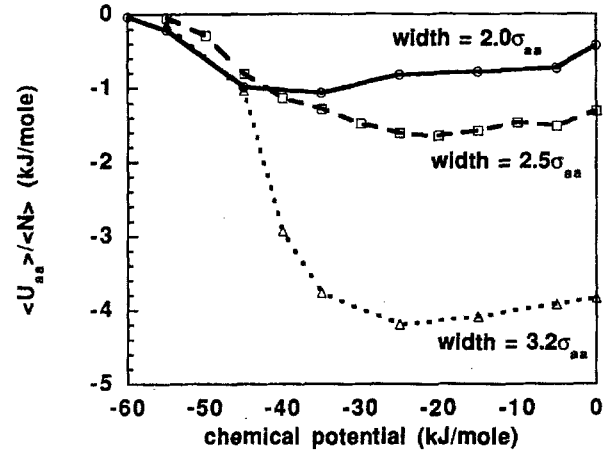


(b)

*Figure 7.* Interaction energies in cylindrical pores as a function of chemical potential. (a) Intensive adsorbate-adsorbate interaction energy, (b) intensive adsorbate-pore interaction energy.

slit pore. From this it is clear that pore curvature and pore size play similar roles. Though greater curvature and smaller pore size strengthen the *ap* interaction and so enhance adsorption at low loading, they also confine the fluid to a greater extent and so retard adsorption at high loadings. Moreover, *aa* repulsion in the cylindrical pore comes into play at lower chemical potentials than in the slit pore because the fluid is more confined in the cylindrical pore now that adsorbates are free only along the axial direction. Although one would expect greater confinement and hence reduced entropy in the cylinder, this is not always the case. In fact, there are higher intensive entropies in a cylindrical pore than in the comparable slit pore because confinement

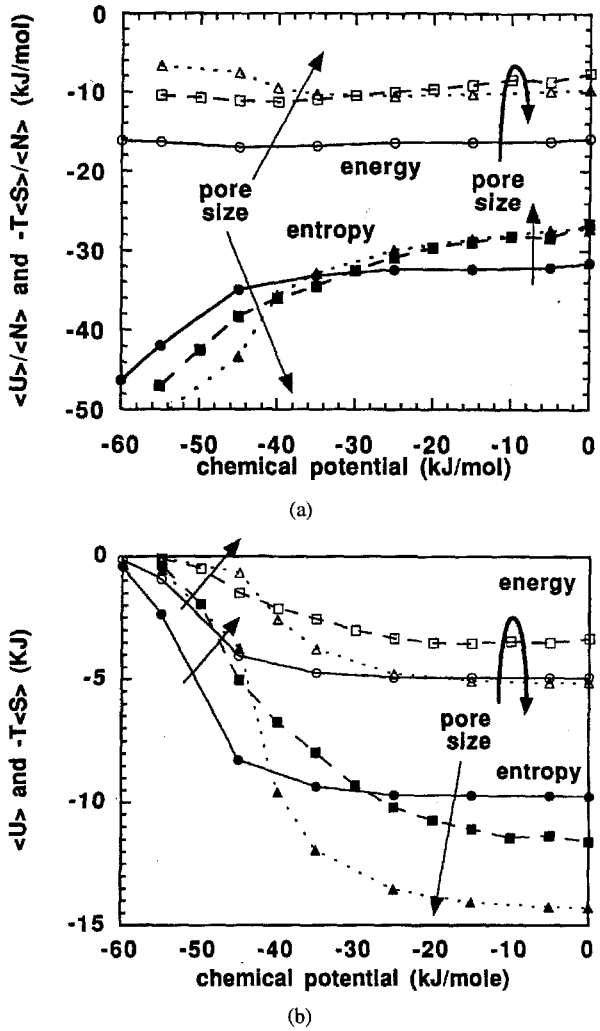


*Figure 8.* Energetic and entropic contributions in cylindrical pores as a function of chemical potential. (a) Intensive energetic and entropic terms, (b) extensive energetic and entropic terms.

in two directions delays the formation of subsequent fluid layers in the cylindrical pore until higher chemical potentials.

*c. **Energetic versus Entropic Effects.*** We find the same contrast between the intensive and extensive thermodynamic properties as we did in the slit pore. The intensive energy always favors the smallest pore. The intensive entropy favors larger pores at low chemical potentials and smaller pores at high chemical potentials.

The extensive properties agree much better with the trends in the isotherms. At low loading, both the extensive energy and entropy favor the smallest pore. At high loading, the extensive entropy now favors the largest pore in agreement with the isotherms. The extensive energy still favors the small pore, so clearly adsorption at high loading is dominated by entropic (packing) effects.

## *C. Spherical Pores*

The adsorption in spherical pores presented here is of course an idealized process since we provide no physical means of entrance or exit. However, such adsorption isotherms can reveal interesting behavior of discrete pores with small entrances. Figure 9 shows the isotherms for Xe in spherical pores of diameter 2.0, 2.5, and $3.2\sigma_{aa}$. The corresponding radial density profiles, *aa* and *ap* interactions, and intensive and extensive energy and entropy are shown in Figs. 10(a,c), 11(a,b), 12(a,b) respectively. The isotherm for the smallest pore has a steep rise and then a distinct plateau that simply represents a maximum loading of one adsorbate per spherical pore. The density profile of the fluid at any chemical potential along the plateau is nearly identical (Fig. 10(a)). The isotherm for the pore of diameter $2.5\sigma_{aa}$ displays two plateaus, the first corresponding to a loading of one Xe per spherical pore and the second to that of two Xe. The density profiles at the two plateaus are markedly different (Fig. 10(b)). These steps in the isotherms were not observed in slit or cylindrical pores simply because those pores were continuous in at least one direction, allowing a greater variety of configurations in the ensemble. The largest spherical pore, which can hold up to six adsorbates,

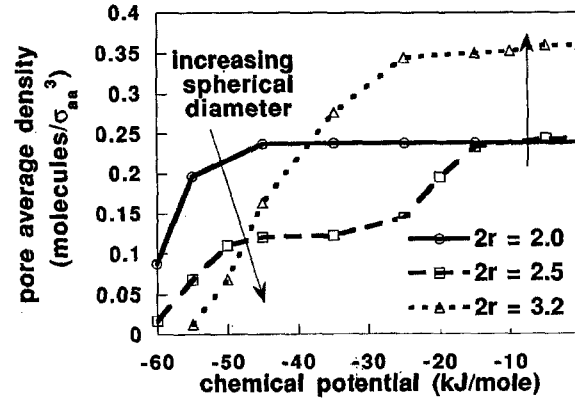


*Figure 9.* Isotherms for spherical pores of diameter 2.0, 2.5, and 3.2 $\sigma_{aa}$ at $T = 300$ K.

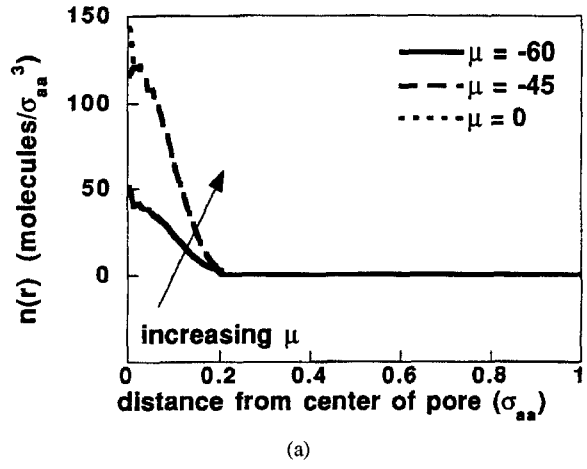


(a)

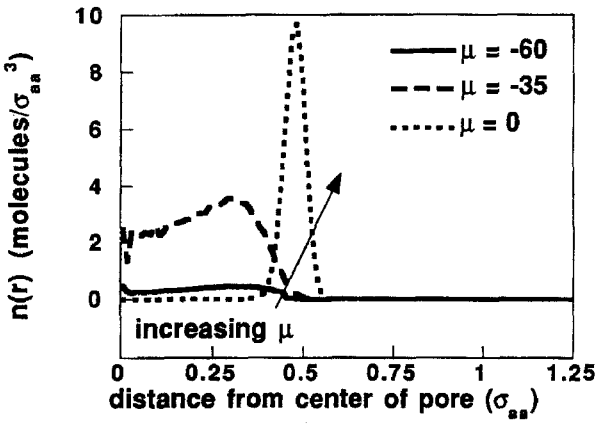


(b)

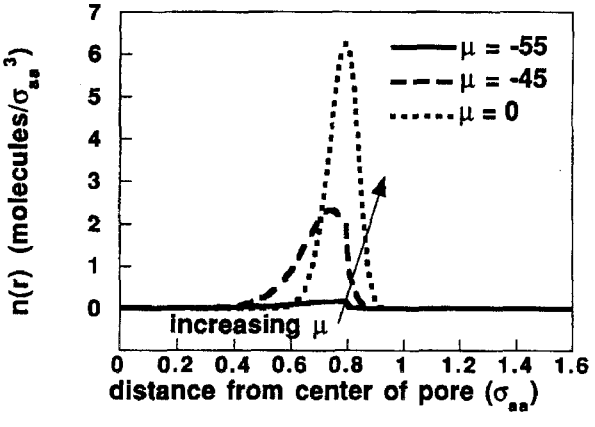


(c)

*Figure 10.* Radial density profiles in spherical pores for several values of the chemical potential. (a) Spherical diameter $= 2.0\sigma_{aa}$, (b) spherical diameter $= 2.5\sigma_{aa}$, (c) spherical diameter $= 3.2\sigma_{aa}$.

shows no distinct steps since the filling process is more gradual.

*a. Low Loadings ($\mu \leq -45$ kJ/mole).* As in the slit and cylindrical pores, at low loading the smallest spherical pore favors adsorption. Again this trend is due to greater *ap* attraction in the smaller pore and negligible *aa* interactions (Fig. 11(1–b)). Also, as was the case in the other two pore shapes, we find the greatest intensive entropy in the largest pores (Fig. 12(a)). The extensive entropy and energy favor the smaller pore.

Comparing adsorption at low loadings in the spherical pores with that in the slit and cylindrical pores,

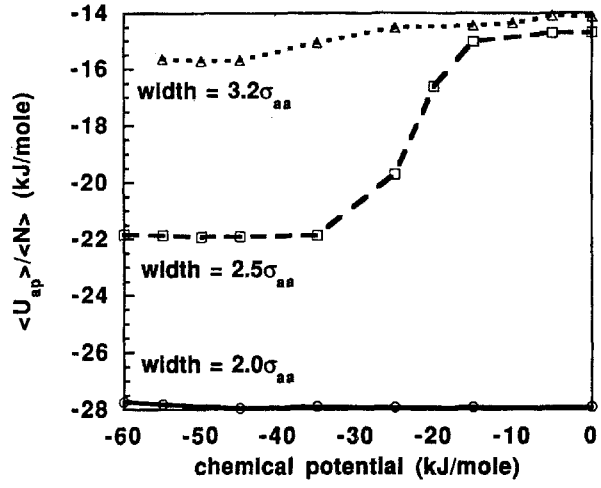


(a)

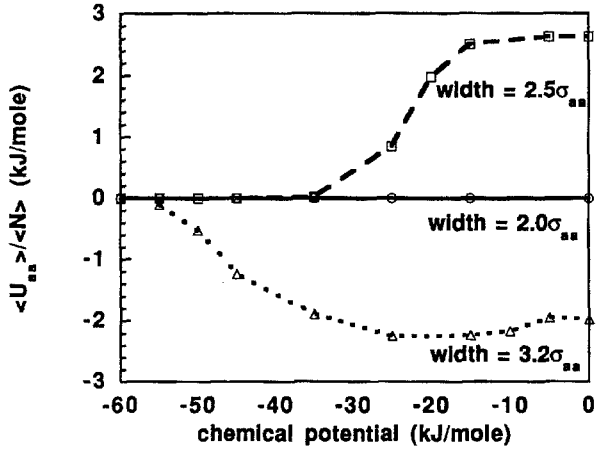


(b)

*Figure 11.* Interaction energies in spherical pores as a function of chemical potential. (a) Intensive adsorbate-adsorbate interaction energy, (b) intensive adsorbate-pore interaction energy.

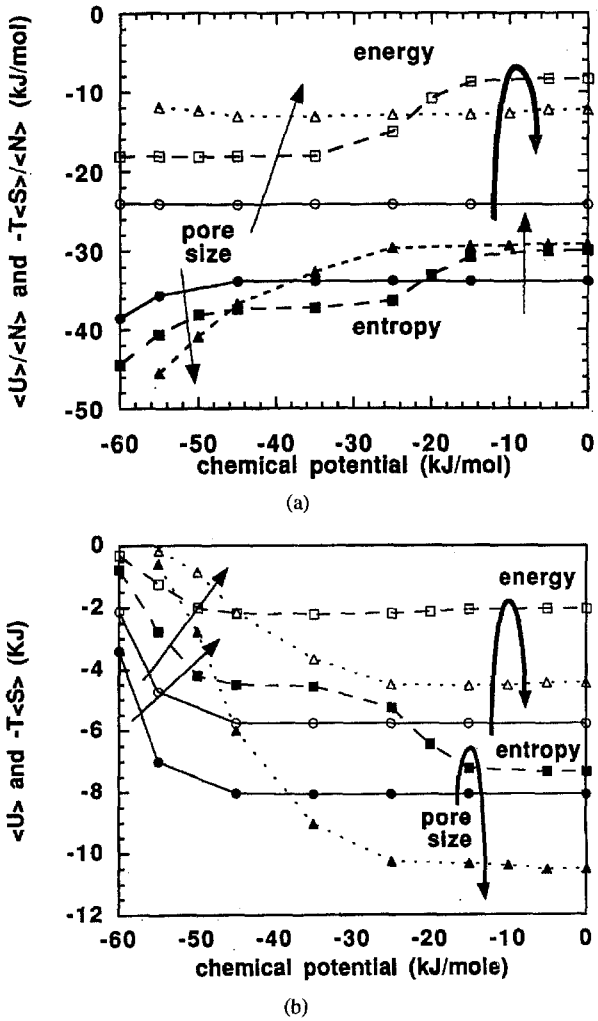


*Figure 12.* Energetic and entropic contributions in spherical pores as a function of chemical potential. (a) Intensive energetic and entropic terms, (b) extensive energetic and entropic terms.

we find that adsorption is favored in the spherical pore. This continues the trend observed in moving from the slit to the cylinder that increasing pore curvature has the same effect as decreasing pore size, specifically, strengthening the *ap* attraction.

***b. High Loadings ($\mu \geq -15$ kJ/mole).*** At high loadings, we again observe that the largest pore displays the greatest adsorption. An additional cause for this reversal in the very confined spherical pores is that the smaller pores allow at most one or two adsorbates. A plot of the *aa* interaction energy with pore size shows much different behavior than that in the previous pore shapes. In the smallest pore, the *aa* energy is zero at all loadings since the maximum occupancy of a single pore is one adsorbate and there is no inter-pore *aa* interactions. In the intermediate sized pore, though, as soon as two adsorbates occupy the same pore, the *aa* interaction is repulsive because the pore can accommodate both adsorbates only by situating them close together. In the largest pore, the *aa* interaction is attractive, as was the case in the slit and cylindrical pores. (Moreover, the *ap* interaction of the intermediate-sized pore is less attractive as the adsorbates are forced into less favorable regions of the pore.)

At high loading, the entropy shows a long plateau for the smallest pore where adsorption is limited to 1 adsorbate per spherical pore. The entropy shows two short plateaus in the intermediate pore because only 1 or 2 adsorbates can simultaneously adsorb. As was the case for the slit and cylindrical pores, the intensive entropy is smaller for the larger pore. However, now we see that the extensive entropy is non-monotonic with respect to spherical pore size. This is a result of the discrete spherical pores of diameter 2.0 and $2.5\sigma_{aa}$ having limits of 1 and 2 adsorbates per pore (which do not allow the increase in density with increasing chemical potential to balance the decrease in intensive entropy).

At $-30$ kJ/mol, we find a non-monotonic trend in adsorption versus spherical pore size; the largest pore most favors adsorption followed by the smallest pore then the intermediate pore. The extensive entropy and energy both favor this trend. At $-30$ kJ/mol, the intermediate pore contains, on average, one adsorbate so, energetically, there is no *aa* attraction and, entropically, although the intensive entropy is greatest in this pore, the density is lowest, thus the extensive entropy does not favor it.

At high loadings, the spherical pore adsorbs less than the slit or cylindrical pores. This too is consistent with the trend that greater confinement retards adsorption at high loadings.

***c. Energetic versus Entropic Effects.*** The intensive energetic and entropic terms are closer in magnitude in the spherical pore than in the slit or cylindrical pores, in part due to the deeper potential wells of the spherical pore, which increases the energetic term and decreases the entropic term.

Again, the intensive and extensive thermodynamic properties show different trends for adsorption with pore size (Fig. 12(a,b)). As was the case in the slit and the cylindrical pore, at low loadings, both the extensive entropic and energetic terms favor adsorption in

the smallest pore. At high loadings, though, the extensive entropic term favors the largest pore, the smallest pore, and then the intermediate pore while the energetic term favors the smallest pore, then the largest pore, then the intermediate pore. Again it is the extensive entropy which best correlates with the isotherm. The isotherm, however, shows adsorption strictly increases with pore size, agreeing with neither the energetic nor entropic term. It is, however, closer to the entropic term. From this we see that the extensive variables (in addition to the intensive variables) cannot fully account for the differences due to the different accessible volumes of the pore.

### D. *Effect of Pore Size and Shape at Selected Chemical Potentials*

Up to now, we have focused on a few given pore sizes while allowing a wide range of chemical potentials so that we could calculate both energetic and entropic terms. In view of the above results, though, it is now instructive to select typical high and low chemical potentials and vary pore size more smoothly.

In Fig. 13(a), we show the density of the adsorbed fluid in a wide range of slit, cylindrical, and spherical pore sizes at chemical potentials of $-45$ and $-15$ kJ/mol. We can explain the features in these isotherms based on the arguments presented above. At the low chemical potential, adsorption decreases as pore size increases because the *ap* interaction weakens with increasing pore size. The spherical pore shows a small rise in loading and then decreases again. The rise is due to the onset of multiple adsorbate molecules being able to enter the larger pores. In general, the spherical pore adsorbs more than the cylindrical pore, which in turn adsorbs more than the slit pore, due to the increasing *ap* attraction with pore curvature. As all the pores become larger, the densities are falling to the bulk value of 0.0014 molecules/$\sigma_{aa}^3$.

At the high chemical potential, oscillations appear in the density as a function of pore size for all pore shapes. Each rise in the density reflects the formation of a new layer in the pore. Overall, the densities increase with increasing pore size, tending toward the bulk value of 0.935 molecules/$\sigma_{aa}^3$. The density increases with pore size due to the decrease in confinement, which results in (i) higher entropies and (ii) more attractive *aa* interactions. Similiarly, the density increases as pore curvature decreases from spherical to cylindrical to slit pore.

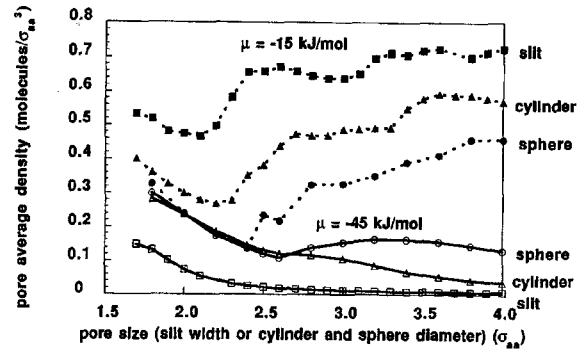


(a)

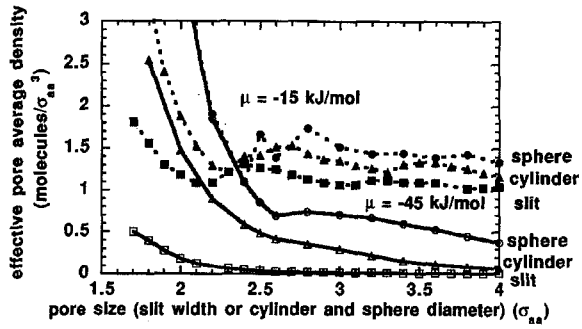


(b)

*Figure 13.* Adsorption in slit, cylindrical, and spherical nanopores over a range of pore sizes from 7 to 16 Å at chemical potentials of $-45$ and $-15$ kJ/mol. (a) Density, (b) effective density.

## 4. Summary

We have shown adsorption isotherms of Lennard-Jones Xenon as a function of pore size and pore shape for three sizes of slit, cylindrical, and spherical nanopores. We see adsorption favored in smaller pores at low chemical potentials and in larger pores at high chemical potentials. We see adsorption favored in pores with greater curvature at low chemical potentials and in pores with less curvature at high chemical potentials. We have explained the relative favorability of adsorption in terms of the density profiles, the adsorbate-adsorbate and adsorbate-pore interaction energies, and the entropy. At intermediate chemical potentials, the relationships between adsorption and pore size and shape are non-monotonic.

Specifically, at low loadings, where the adsorbate-adsorbate interaction is negligible, the pore with the most favorable external potential will favor adsorption. In smaller and more curved pores, the external potential from adjacent walls can overlap and deepen the potential well, favoring adsorption. In all cases, the

*Table 1.* Accessible volumes.

| Adsorbate/ | L-J/ | L-J/ | H-S/ | L-J/ |
|---|---|---|---|---|
| Adsorbent | L-J | L-J | H-W | L-J |
| Pore size | 2.0 | 2.5 | 2.5 | 3.2 |
| Pore shape | Percent of total volume accessible to absorbate | | | |
| Slit | 40% | 52% | 60% | 62.5% |
| Cylinder | 16% | 27.04% | 36% | 39.06% |
| Sphere | 6.4% | 14.06% | 21.6% | 24.41% |

density was most strongly influenced by the extensive entropy; in fact, at high chemical potential the extensive entropy provided the most serious deviation from ideal gas behavior.

All points raised in individually examining different pore sizes are summarized in Fig. 13(a), bearing in mind the thermodynamic trends shown in Figs. (1–12).

We close this study by suggesting a way to define an effective density in an attempt to explain these trends. We restate that the pore width is defined to be the distance from the plane where the *ap* potential diverges at one point on the pore wall to a similar plane at the point on the opposite side of the pore (what would be, in an atomistically detailed pore, the distance from the center of the first layer of wall atoms to the center of the layer on the opposite side). Not all of the total pore volume is accessible to the adsorbate due to short-range adsorbate-wall repulsion. The distance of closest approach between the adsorbates and the wall at high loading is nearly $0.6\sigma_{aa}$ in all cases. Using this value, we present in Table 1 the accessible volumes in the nine pores studied and a hard-sphere/hard-wall system for comparison. These values indicate that the volume specified in the grand canonical simulation does not give the same accessible volume to pores of different sizes and shapes. We may define an effective density to be the number of molecules in the accessible volume. The isotherms are now shown in terms of the effective density (Fig. 13(b)). The adsorption trends with respect to pore size and shape now remain the same at low loading and at high loading. The smallest, most curved pore has adsorbed the fluid with the greatest effective density at high chemical potentials.

However at high loadings, the simple trend breaks down as the adsorbate packing becomes significant. The importance of adsorbate packing depends upon the geometry of the pore. Spherical pores confine the molecules the most, then cylindrical pores, then slit pores. Adsorption at high chemical potentials is favored in the nanopore with least confinement.

Although this study was confined to a Lennard-Jones fluid and idealized nanopores, we expect elements of similar behavior for more complicated molecules and pores. Because this investigation studied idealized sorbates and pores, the data presented in Figs. 1–13 consumed about 8 hours of CPU time on a Cray XMP. A comparable simulation study in a nanopore with atomistic detail would require an order of magnitude more computer time.

## Nomenclature

| | |
|---|---|
| $k_b$ | Boltzmann constant |
| $n(x)$ | local adsorbate density at position $x$, perpendicular to walls, in slit nanopores |
| $n(r)$ | local adsorbate density at radial position $r$ in cylindrical and spherical nanopores |
| $N$ | number of adsorbate molecules |
| $r_i$ | position of molecule $i$ in pore |
| $r_{ij}$ | distance between molecules $i$ and $j$ |
| $S$ | entropy |
| $T$ | temperature |
| $V$ | volume |
| $U$ | total internal energy |
| $U_{aa}$ | internal energy due to adsorbate-adsorbate interactions |
| $U_{ap}$ | internal energy due to adsorbate-pore interactions |
| $U_{ij}$ | internal energy due to interaction of adsorbates $i$ and $j$ |
| $U_{ip}$ | internal energy due to interaction of adsorbate $i$ and pore |
| $\varepsilon_{aa}$ | Lennard-Jones adsorbate-adsorbate energy parameter |
| $\varepsilon_{ap}$ | Lennard-Jones adsorbate-pore energy parameter |
| $\Lambda$ | de Broglie thermal wavelength |
| $\mu$ | chemical potential |
| $\rho_s$ | density of solid |
| $\sigma_{aa}$ | Lennard-Jones adsorbate collision diameter |
| $\sigma_{ap}$ | Lennard-Jones adsorbate-pore collision diameter |
| $\Omega$ | grand potential |
| $\langle x \rangle$ | ensemble average of $x$ |

## Acknowledgments

We wish to acknowledge the Minnesota Supercomputer Institute, NSF (CTS-9058387), and Union

Carbide for partial support of this work. D. Keffer was partially supported by a Chevron Fellowship.

## References


Allen, M.P. and D.J. Tildesley, *Computer Simulation of Liquids*, Oxford University Press, Oxford, 1987.

Antonchenko, V.Y., V.V. Ilyin, N.N. Makovsky, and V.M. Khryapa, "Short-range Order in Cylindrical liquid-filled Micropores," *Mol. Phys.*, **65**, 1171–83 (1988).

Bratko, D., L. Blum, and M.S. Wertheim, "Structure of Hard Sphere Fluids in Narrow Cylindrical Pores," *J. Chem. Phys.*, **90**, 2752–57 (1989).

Carignan, Y.P., T. Vladimiroff, and A.K. Macpherson, "Molecular Dynamics of Hard Spheres. III. Hard Spheres in an almost Spherical Container," *J. Chem. Phys.*, **88**, 4448–50 (1988).

Davis, H.T., *Statistical Mechanics of Phases, Interfaces, and Thin Films*, VCH, Weinheim, 1995.

Demi, T., "Molecular Dynamics Studies of Adsorption and Transport in Micropores of Different Geometries," *J. Chem. Phys.*, **95**, 9242–47 (1991).

Derouane, E.G., J.M. Andre, and A.A. Lucas,"Surface Curvature Effects in Physisorption and Catalysis by Microporous Solids and Molecular Sieves," *J. Cat.*, **110**, 58–73 (1988).

Dunne, J. and A.L. Myers, "Adsorption of Gas Mixtures in Micropores: Effect of Difference in size of Adsorbate Molecules," *Chem. Eng. Sci.*, **49**, 2941–2951 (1994).

Glandt, E.D., "Density Distribution of Hard-Spherical Molecules inside Small Pores of Various Shapes," *J. Col. Inter. Sci.*, **77**, 512–24 (1980).

Groot, R.D., N.M. Faber, and J.P. van der Eerden, "Hard Sphere Fluids near a Hard Wall and a Hard Cylinder," *Mol. Phys.*, **62**, 861–74 (1987).

Han, K.K., J.H. Cushman, and D.J. Diestler, "Grand Canonical Monte Carlo Simulations of a Stockmayer Fluid in a Slit Micropore," *Mol. Phys.*, **79**, 537–45 (1993).

Heinbuch, U. and J. Fischer, "Liquid Argon in a Cylindrical Carbon Pore: Molecular Dynamics and Born-Green-Yvon Results," *Chem. Phys. Let.*, **135**, 587–90 (1987).

Jiang, S., C.I. Rhykerd, and K.E. Gubbins, "Layering, Freezing Transitions, Capillary Condensation, and Diffusion of Methane in Slit Carbon Pores," *Mol. Phys.*, **79**, 373–91 (1993).

Macelroy, J.M.D. and S.H. Suh, "Computer Simulation of Moderately Dense Hard-Sphere Fluids and Mixtures in Microcapillaries," *Mol. Phys.*, **60**, 475–501 (1987).

Macelroy, J.M.D. and S.H. Suh, "Simulation Studies of a Lennard-Jones Liquid In Micropores," *Mol. Sim.*, **2**, 313–351 (1989).

Macpherson, A.K., Y.P. Carignan, and T. Vladimiroff, "Molecular Dynamics of Hard Spheres. II. Hard Spheres in a Spherical Cavity," *J. Chem. Phys.*, **87**, 1768–70 (1987).

Murad, S., P. Ravi, and J.G. Powles, "A Computer Simulation Study of Fluids in Model Slit, Tubular, and Cubic Micropores," *J. Chem. Phys.*, **98**, 9771–81 (1993).

Peterson, B.K., J.P.R.B. Walton, and K.E. Gubbins, "Fluid Behaviour in Narrow Pores," *J. Chem. Soc., Faraday Trans. 2*, **82**, 1789–1800 (1986).

Peterson B.K. and K.E. Gubbins, "Phase Transitions in a Cylindrical Pore: Grand Canonical Monte Carlo, Mean Field Theory, and the Kelvin Equation," *Mol. Phys.*, **62**, 215–26 (1987).

Saito, A. and H.C. Foley, "Curvature and Parametric Sensitivity in Models for Adsorption in Micropores," *AIChE J.*, **37**, 429–36 (1990).

Sarman, S., "The Influence of the Fluid-Wall Interaction Potential on the Structure of a Simple Fluid in a Narrow Slit," *J. Chem. Phys.*, **92**, 4447–55 (1990).

Schoen, M., C.L. Rhykerd, J.H. Cushman, and D.J. Diestler, "Slit-pore Sorption Isotherms by the Grand-Canonical Monte Carlo Method: Manifestations of Hysteresis," *Mol. Phys.*, **66**, 1171–87 (1989).

Somers, S.A. and H.T. Davis, "Microscopic Dynamics of Fluids Confined between Smooth and Atomically Structured Solid Surfaces," *J. Chem. Phys.*, **96**, 5389–407 (1992).

Somers, S.A., A.V. McCormick, and H.T. Davis, "Superselectivity and Solvation Forces of a Two Component Fluid Adsorbed in Nanopores," *J. Chem. Phys.*, **99**, 9890–8 (1993).

Tan, Z. and K.E. Gubbins, "Selective Adsorption of Simple Mixtures in Slit Pores: A Model of Methane-Ethane Mixtures in Carbon," *J. Phys. Chem.*, **96**, 845–54 (1992).

Van Tassel, P.R., H.T. Davis, and A.V. McCormick, "Open-system Monte Carlo simulations of Xe in NaA," *J. Chem. Phys.*, **98**, 8919–28 (1993).

Walton, J.P.R.B. and N. Quirke, "Capillary Condensation: A Molecular Simulation Study," *Mol. Sim.*, **2**, 361–91 (1989).